Review Paper

Diagnostics of Recombining Plasmas in Divertor Simulator MAP-II*

KADO Shinichiro[1)], IIDA Yohei[2)], KAJITA Shin[2)]**, YAMASAKI Daisuke[2)], OKAMOTO Atsushi[1)]***, XIAO Bingjia[3)], SHIKAMA Taiichi[2)], OISHI Tetsutaro[2)] and TANAKA Satoru[2)]

[1)]*High Temperature Plasma Center, The University of Tokyo, Kashiwa, Chiba 227-8568 JAPAN*

[2)]*School of Engineering, The University of Tokyo, Tokyo 113-8656 JAPAN*

[3)]*Institute of Plasma Physics, Chinese Academy of Sciences, P O Box 1126, Hefei, Anhui 230031, P R China*

(Received 22 March 2005 / Accepted 25 August 2005)

Atomic and molecular processes in volumetric recombination phenomena relevant to divertor detachment are investigated in a divertor simulator MAP (Material and Plasma) -II. In the recombining plasmas, quantitative measurements of parameters, especially using a Langmuir probe, are difficult, so that the development of alternative diagnostics is important. Recombination can be induced in He plasma by puffing of He or H_2. In the He puffing case, the Rydberg spectra show an electron temperature of lower than 0.1 eV, while in the H_2 puffing case, the Rydberg spectra disappear even though the reduction of the ion flux is apparent, showing that another type of recombination occurs. Negative hydrogen ions are observed in the peripheral region of the plasma column.

Keywords:

divertor simulator, MAP-II, detachment, volumetric recombination, recombining plasma, negative ion, laser photodetachment, Fulcher band, collisional-radiative model

1. Introduction

Enhancement of recombination processes in the plasma volume to achieve a detached plasma is one of the most promising scenarios for the reduction of particle and heat fluxes onto the divertor plate in magnetic confinement fusion devices. In order to cool the divertor/edge plasmas, especially electrons, towards the recombination regime, where the momentum of the plasma is not conserved along the magnetic field, fuelling gases H_2 or D_2, or more actively, rare gases such as Ne or Ar, are puffed into the divertor region as radiators [1].

In addition to conventional electron-ion recombination processes characterized by radiative and three-body recombinations, molecular assisted/activated recombination (MAR) processes induced by the hydrogen [2] or hydrocarbon [3] puffing recently have been revealed to have the capability to contribute to the volumetric recombination. The conditions for each process to be effective strongly depend on the plasma parameters, such as electron temperature T_e and electron density n_e. Therefore, it is important to apply reliable diagnostics to investigate detached recombining plasmas.

One difficulty in investigating recombining detached plasmas is the anomaly in the Langmuir probe current (I)-voltage (V) characteristics as reported in refs. [4-6]. The measured value of T_e "appears" to increase as ion flux decreases due to recombination, even though there is no apparent mechanism of heating. Another difficulty is in the determination of the lowest principal quantum number of the Rydberg states above which atomic Boltzmann plot method can be performed for the measurement of the electron temperature.

For the purpose of exploring plasma-wall or plasma-gas interaction in the divertor/edge region, steady-state linear plasma devices, which simulate the open magnetic field from the scrape-off layer (SOL) to the divertor plate, have been regarded as useful. Many machines are operating following this concept, such as the Plasma Interaction Surface Component Experimental Station (PISCES)-A [7] and -B [8] in UCSD (USA), PSI-2 [9] in IPP-Berlin, LENTA [10] in the Kurchatov Institute (Russia), the UMIST linear system (ULS) [11] in UMIST (UK), the Test Plasma by Direct Current (TPD)-II [12] in NIFS (Japan), Nagoya Divertor Simulator (NAGDIS)-I [13] and -II [14] in Nagoya Univ. (Japan) or TPDSHEET-IV [15] in Tokai Univ. (Japan).

Our first generation single-chamber device, MAP (material(s) and plasma), was developed by Bolt and Tanaka for the purpose of investigating mainly material erosion phenomena by plasma irradiation in about 1990 [16-21] in the Tokai-mura site of the University of Tokyo. MAP was

author's e-mail: kado@q.t.u-tokyo.ac.jp

**This paper was presented as an invited talk at the 21st annual meeting of the Japan Society of Plasma Science and Nuclear Fusion Research, Nov. 23-26, 2004, Shizuoka, Japan, 24aB01.*

*Present affiliation: **Graduate School of Engineering, Nagoya University. ***Graduate School of Engineering, Tohoku University*

modified to a dual-chamber device MAP-II in 1999, which enabled the gas-target experiments and expanded the controllability of the discharge conditions [22]. Stabilized power supplies and a full turbo molecular pumping system have been applied from 2001. Consequently, the time invariance and the reproducibility of the plasma parameters have been improved to a great extent.

In the present paper, we first review the atomic and molecular processes relevant to the divertor detachment and the spectroscopic methods used to observe them in Sec. **2**. In Sec. **3**, we describe the detailed apparatus of the MAP-II device and the diagnostics installed for the purpose of investigating the key phenomena in each recombination processes. Then, measurements of Rydberg spectra in electron-ion recombination (EIR) plasmas and negative ions in H_2-MAR plasmas, together with the vibrational distribution of the molecular hydrogen, are reviewed in Sec. **4**. The paper concludes with a summary and a discussion of future prospects.

2. Atomic and Molecular Processes Relevant to Divertor Plasma Detachment and their Diagnostics

2.1 Electron-Ion Recombination (EIR)

2.1.1 Atomic boltzmann plot method

General volumetric recombination processes, EIR, are categorized into:

(a) $e + A^+ \rightarrow A(n = p) + h\nu$
: radiative recombination (RR),

(b) $e + e + A^+ \rightarrow A(n = p) + e$
: three-body recombination (3BR),

where n represents the principal quantum number. In the case of a free-electron being captured into an $n = p$ excited state, both processes can emit a line spectrum as

$A(n = p) \rightarrow A(n = q) + h\nu_{q \leftarrow p}$: radiative decay,

where $p > q$. These recombination processes overcome the ionization processes under high density (typically $\geq 10^{13}$ cm^{-3}) and low temperature (typically ≤ 1 eV) conditions.

The spectral intensities $I_{q \leftarrow p}$ from the upper energy level E_p can be represented, in thermal equilibrium plasmas, by the natural logarithmic form,

$$\ln\left(\frac{I_{q \leftarrow p}\lambda_{q \leftarrow p}}{g_p A_{q \leftarrow p}}\right) = \text{const} - \frac{E_p}{kT_e}, \qquad (1)$$

where $A_{q \leftarrow p}$ and $\lambda_{q \leftarrow p}$ denote the spontaneous emission coefficient and the wavelength of the $n = p$ to q transition, respectively, while g_p is the statistical weight in the upper state p and k is the Boltzmann constant. The argument of the natural logarithm is proportional to the population density per degeneracy of the p state. Since the Rydberg state electrons can easily achieve the partial local thermal equilibrium (p-LTE) with free electrons, plots of the left-hand side of Eq. (1) show a linear dependence on E_p, at least in highly excited states. Because the emission intensity of the EIR spectra depends on the electron density n_e and the electron temperature T_e, the line-integral intensities are weighted by the intensity profile. Therefore, from the reciprocal of the slope, this so-called atomic Boltzmann plot method yields T_e at the brightest point (usually the low temperature peripheral region is brighter) [23,24].

In passive spectroscopy, the Rydberg spectra can only be observed when sufficient electrons are supplied to the p-LTE states. Hence, the presence of the Rydberg spectra can be regarded as indicative of the EIR phenomena.

2.1.2 Collisional-radiative model

In the atomic Boltzmann plot, determination of the lowest n usable for the fitting procedure is ambiguous. This is because the negative slope gradually decreases as the lowest n chosen decreases. Application of a collisional-radiative (CR) model is an alternative method to find the best-fit line intensity ratio which is dependent on the plasma parameters. In this case, a reliable atomic data set, especially for electron-impact excitation and de-excitation cross-sections, is indispensable.

The CR model for the neutral Helium line (He I) was developed by Fujimoto [25] and updated by Goto [26]. We made a modification to Goto's code to deal with the radiation trapping in the cylindrical geometry of the MAP-II plasmas based on Otsuka's formulation [27], as described in Sec. **4.1**.

In the CR model for He I, the population density of the $n = p$ state for a given T_e and n_e can be written as:

$$n(p, T_e, n_e) = r_0 n_e n_i + r_1 n_e n(1^1S) + r_2 n_e n(2^1S) + r_3 n_e n(2^3S), \qquad (2)$$

where $r_i (i = 0, 1, 2, 3)$ represent population coefficients which describe the contribution from the population densities of ionic, ground 1^1S, meta-stable 2^1S and meta-stable 2^3S states, respectively. In the recombining plasma, the last three terms become negligible and the population ratio can be determined only from r_0.

2.2 Molecular-assisted recombination (MAR)

2.2.1 Observation of the MAR phenomena

Hydrogen (H_2)-MAR (Molecular Assisted/Activated Recombination) process enhanced by vibrationally excited molecular hydrogen can dominate the plasma extinction in the electron temperatures of about 1–3 eV. These temperatures are higher than those for the EIR process. The following processes are identified:

(c) $H_2(v) + e \rightarrow (H_2^-)^* \rightarrow H^- + H$
: Dissociative Attachment (DA) [28]
followed by $H^- + H^+ \rightarrow H + H^*$
: Mutual Neutralization (MN)

(d) $H_2(v) + A^+ \rightarrow (AH)^+ + H$
: Ion Conversion (IC) [29]
followed by $(AH)^+ + e \rightarrow A + H^*$
: Dissociative Recombination (DR)

(e) $H_2(v) + A^+ \rightarrow H_2(v)^+ + A$
: Charge Exchange Ionization (CX)
followed by $H_2^+ + e \rightarrow H + H^*$
: DR

where A represents a neutral atom, such as H, He or Ar, while v denotes the vibrational quantum number. The distribution

of the vibrational quantum state is often attributed to the Boltzmann vibrational temperature T_{vib}. Usually, (d) has a larger reaction rate than (e) [30] although in the case of A being H, they are not distinguishable. In channel (c), negative hydrogen ions play an important role in recombination processes [28,29].

Observations of the atomic and molecular processes which dominate H_2-MAR rely on the measurement of H*, H^- and $H_2(v)$. The excited state population of H*, especially n = 2–4, is evaluated from the deviation from the calculation results obtained using a CR model without taking MAR into consideration [31]. The H^- density can be measured using the laser photodetachment (LPD) method [32] as described below. Furthermore, it is desirable to measure the density of $H_2(v)$ at the same time.

2.2.2 Combined scheme of the eclipse laser photodetachment method and the double probe for negative hydrogen ions in detached plasmas

The negative ion density can be measured based on the following photodetachment process due to the laser photon which has an energy hv:

(g) $H^- + hv \rightarrow H + e$: Photodetachment (PD).

Excess electrons released from the negative ions correspond to the negative ion destroyed due to laser injection. To collect these electrons, an L-shaped electrostatic probe with a positive bias, V_p, is commonly used so that its interaction surface with the laser channel is long. Because the sensitivities of the electron current, I_e, to the electron density, n_e, at the space potential, V_s, and at the positive bias, V_p, can be regarded as equal, the following simple formula can apply in the case of using a laser operating at the saturation pulse energy density of process (g):

$$\frac{\Delta I_e(V_p)}{I_e(V_p)} = \frac{\Delta I_e(V_s)}{I_e(V_s)} = \frac{\Delta n_e}{n_e} = \frac{n_-}{n_e}, \tag{3}$$

where n_e is determined from the I-V characteristics of the single probe together with T_e.

Bacal first applied this method to the plasmas containing negative hydrogen ions [32]. It has been followed by a considerable number of theoretical and experimental studies on the interpretation of the waveform of the LPD signal detected by a probe, through the development of so-called negative ion sources (see ref. [33] and the references therein). Recently, since much attention has been paid to the role of negative ions in plasma recombination, the LPD method has also been applied to the divertor simulators such as MAP-II [34] and TPDSHEET-IV [15]. A common characteristic of the negative ions in the divertor-simulating discharge plasmas is that they localize in the peripheral region of the plasma column where the electron temperature is low (the details are described in Sec. **4.2**).

In the application of the laser photodetachment (LPD) method to divertor plasmas, we have identified three difficulties:

1) an anomaly in the probe characteristics [4-6],
2) ablation of the probe surface adsorbates which are ionized due to the electron impact processes [35], and
3) the effect of the magnetic field.

The item 1) disturbs the T_e measurement which is necessary for the determination of n_e in Eq. (3). Consequently, n_e deduced from the electron current does not correspond to the electron density.

For the purpose of compensating for the single probe anomaly, one should return to the direct relationship between the excess electron density, Δn_e, and the excess electron current, ΔI_e, at the space potential V_s, given as:

$$\Delta I_e(V_s) = \frac{eS}{4}\Delta n_e\sqrt{8kT_e/\pi m_e}, \tag{4}$$

where S is the probe surface area and m_e is the electron mass. In this equation, T_e should be approximated by a plausible value [36]. We assume that the anomaly appears only in the bulk electron current and not in the excess electron current, since the excess electron swarm is produced at a quite short distance from the probe. In fact, the collection region for the photodetached electron is smaller than the laser radius in our experimental regime [37].

Another ambiguity in Eq. (4) is the difference between the probe bias V_p and the space potential V_s (usually $V_p > V_s$). It may safely be assumed, however, that the degree of electron current reduction due to the plasma impedance or potential bursts [6] does not depend on the probe bias voltage. Therefore, we have the following more direct representation:

$$\frac{\Delta I_e(V_p)}{I_e(V_p)} = \frac{\frac{eS}{4}\Delta n_e\sqrt{8kT_e/\pi m_e}}{I_e(V_s)}. \tag{5}$$

It has been reported that the double probe provides more reliable values in detached recombining plasmas [6]. Therefore, if T_e in the equation is measured by a double probe at the same position, the negative ion density can be obtained [38].

Concerning item 2), the superposition of the probe surface ablation signal onto the photodetached excess electron current leads to an overestimation of the negative ion density even using a laser pulse energy density lower than the saturation pulse energy density of the PD process (typically 50 mJ/cm^2 for 532 nm). This is especially true when the electron density is high and when gases other than hydrogen, such as helium, hydrocarbons or their mixture with hydrogen are used. Ablation phenomena can be detected by a negatively biased probe since ions are also produced through the ionizations of neutrals whereas no ions are produced through the PD process. We have revealed that the ablation occurs from the loss of the thermal balance between the adsorbing/implanting and desorbing/released contaminants [35]. Formation of helium blisters may be an enhancement factor. In fact, using an *in-situ* heated probe, the ablation phenomena are reduced and the use of pure hydrogen gas increases the threshold pulse energy density for the onset of ablation up to several hundred mJ/cm^2 [39]. This is due to the fact that in a pure hydrogen

discharge, cleaning of the probe surface through hydrogen chemical reactions overcomes contamination.

For the purpose of actively avoiding the ablation phenomena, we have developed a novel method called Eclipse-LPD [40]. A thin wire is installed in the laser channel to shield the probe tip from the irradiation of the laser pulse, just as the earth shields the moon from the irradiation of the sunlight during a lunar eclipse. This method also has the capability of measuring the thicknesses of the electron sheath and the collection region of photodetached electrons (PDE's), which are described in detail in ref. [37]. The collection region of the PDE's can be defined by the minimum laser diameter which can supply enough excess electrons to the probe circuit. In other words, the signal cannot reach its peak corresponding to the negative ion density if a laser diameter is smaller than the collection region. Because the collection region of PDE's might be elongated due to the existence of the magnetic field (item 3), it is important to check if the laser diameter is larger than the collection region of the PDE's measured using the Eclipse-LPD.

For the measurement of the negative ions in the detached recombining plasmas, we have proposed the combined scheme of the Eclipse-LPD and the double probe, in which T_e in Eq. (5) is measured with the double probe mounted in the same probe head as the L-shaped probe for the Eclipse-LPD.

2.2.3 Fulcher-band spectroscopy for $H_2(v)$

Most direct emission spectroscopy to obtain the vibrational distribution in the ground electronic state of molecular hydrogen, $X^1\Sigma_g^+$, is the one by which the radiative decay from the $B^1\Sigma_u^+$ or $C^1\Pi_u$ state is measured [41]. However, these wavelengths are in the vacuum ultraviolet (VUV) region and installing the measurement system in the divertor region is complicated. In contrast, the Fulcher-α system, $d^3\Pi_u \rightarrow a^3\Sigma_g^+$, has a relatively strong intensity in the visible region, so that it has been applied as an indirect measurement of the vibrational distribution, although only the vibronic state up to $v' = 3$ can be measured due to the predissociation of the $d^3\Pi_u$ state.

The Fulcher-band spectroscopy has been employed for the indirect determination of the gas temperature of technical plasmas [42]. In the mid-90s, Fantz applied this method to microwave discharge plasmas [43] and then to the divertor region of the ASDEX-U Tokamak [44], which received considerable attention because of its importance in the study of the vibrational distribution of the molecular hydrogen in the divertor/edge plasmas. Because it is known that the intensities of the P and R branches in the ro-vibronic Fulcher transitions do not follow the Hönl-London branching ratio (i.e., "irregular" intensity ratio), whereas the Q branch exhibits a "regular" intensity ratio [45], the Q branch spectra have been used in the analysis.

We have developed in ref. [46] an analysis method by assuming the ground state ($X^1\Sigma_g^+$) Boltzmann populations both for vibrational (v) and rotational (J) distributions, which correspond to the equivalent temperatures, $T_{\rm vib}^X$ and $T_{\rm rot}^X$, respectively,

$$N_{XvJ} = C_v(2J+1)g_{as}^J \exp\left[-\frac{F_X(J,v)}{kT_{\rm rot}^X} - \frac{G^X(v)-G^X(0)}{kT_{\rm vib}^X}\right], \quad (6)$$

where C_v is a normalization constant to satisfy the requirement that the sum of the Eq. (6) with respect to J gives the vibrational population N_{Xv}. The degeneracy of the nuclear spin g_{as}^J stands for "asymmetric" or "symmetric" depending on the symmetry of the level J. In H_2, levels of odd J in $d^3\Pi_u^-$ (Q branches) and in $X^1\Sigma_g^+$, and of even J in $d^3\Pi_u^+$ (P and R branches) are asymmetric, so that the wave function of the nuclear spin is symmetric to satisfy the features of fermions, *i.e.* $g_{as}^J = g_s^a = 3$, while the opposite case requires $g_{as}^J = g_a^s = 1$. $F_X(J, v)$ and $G_X(v)$ are the rotational and vibrational energies in the $X^1\Sigma_g^+$ state, respectively.

By using the electron impact excitation rate from the $X(v, J)$ to the $d(v', J')$ state, $R_{XvJ}^{dv'J'}$, and the spontaneous emission coefficient from the $d(v', J')$ to the $a(v'', J'')$ state, $A_{av''J''}^{dv'J'}$, in the coronal equilibrium, the measured line intensities having the wavelength $\lambda_{av''J''}^{dv'J'}$ can be expressed by the following fitting function to obtain $T_{\rm vib}^X$ and $T_{\rm rot}^X$:

$$I_{av''J''}^{dv'J'} = \frac{hc}{\lambda_{av''J''}^{dv'J'}} \frac{A_{av''J''}^{dv'J'}}{\sum_{v'',J''} A_{av''J''}^{dv'J'}} \times n_e \sum_{v,J} \left\{ R_{XvJ}^{dv'J'} C_v(2J+1) g_{as}^J \exp\left[-\frac{F_X(J,v)}{kT_{\rm rot}^X} - \frac{G_X(v)-G_X(0)}{kT_{\rm vib}^X}\right]\right\}, \quad (7)$$

where h and c are the Planck constant and the light velocity, respectively.

The ro-vibronic structure of $A_{av''J''}^{dv'J'}$ for the diagonal band can be well described by the Franck-Condon factor $q_{v'v''}$ [43] and the Hönl-London factor for the P, Q or R branch, namely,

$$S_{J'J''}^P = J'/2, \quad S_{J'J''}^Q = (2J'+1)/2, \quad S_{J'J''}^R = (J'+1)/2. \quad (8)$$

Note that

$$S_{J'J''}^Q = S_{J'J''}^P + S_{J'J''}^R = (2J'+1)/2. \quad (9)$$

The ro-vibrational structure in the excitation rate $R_{XvJ}^{dv'J'}$ is evaluated from the adiabatic approximation [47] combined with Gryzinski's semi-classical electron exchange cross-sections [48]:

$$R_{XvJ}^{dv'J'} = q_{Xv}^{dv'} < Q_{v'\leftarrow v}^{\rm Gryzinski} v_e > a_{0J}^{1J'} \delta_{g_{as}^J}^{g_{as}^{J'}},$$

$$\sum_{K'} a_{\Lambda K}^{\Lambda' K'} = \sum_{K'} \sum_r \bar{Q}_r' (2K'+1) \begin{pmatrix} K' & r & K \\ \Lambda' & \Lambda-\Lambda' & -\Lambda \end{pmatrix}^2 = 1, \quad (10)$$

where $\bar{Q}_r'$ are the multi-polar components of the partial cross-section determined in ref. [47], which are 0.76, 0.122, 0.1, and 0.014 for r = 1~4. Note that the dipolar component of $a_{0J'}^{1J'}$, namely, $\bar{Q}_1'$ with $r = 1$ corresponds to the Hönl-London factor for the X to d transition. Kronecker's delta represents

the selection rule for the symmetry of the nuclear spin. The spin multiplicity is so small that the rotational quantum number without spin, *K,* can be replaced by *J* in this case.

It has been confirmed that the upper Fulcher state populations deduced from this fitting function are consistent with the value obtained from the conventional way in which the upper state rotational distributions are fit to the rotational temperature using the molecular Boltzmann plot method for each vibronic state, $T_{\mathrm{rot}}^{dv'}$, namely,

$$N_{dv'} = \frac{N_{dv'}(1)}{(2\cdot 1+1)\cdot g_s^a}\sum_{J'\geq 1}(2J'+1)g_{as}^{J'}\exp\left[-\frac{F_{dv}(J')-F_{dv}(1)}{kT_{\mathrm{rot}}^{dv'}}\right], \tag{11}$$

if the same $R_{XvJ}^{dv'J'}$ and $A_{av''J''}^{dv'J'}$ are used. So the conventional way also applies although the usable vibronic lines to determine T_{vib}^X are limited to 4. One of the merits in our fitting scheme to determine T_{rot}^X and T_{vib}^X is that many lines, say about 14, can be used so that the results are less influenced by the line contamination or noise.

Through this procedure, we have revealed, that the sum of the P and R branches exhibits "regular" intensity ratio while the rotational temperature is still anomalous [49,50]. In the present analysis, therefore, we also used only the Q branch spectra in the ro-vibrational analysis of the Fulcher-band.

A CR model is applied to the H atom. The code used in the present study is the simplest one in which only hydrogen atoms can be treated. The dissociative excitation rate of H_2 scales as the inverse power of 6 of the principal quantum number n while the direct electron impact excitation rate of H atoms scales as the inverse power of 3 [51]. This suggests that the molecular contribution to the Balmer series emission decreases as n increases. Therefore, the ratio of H atomic to H_2 molecular densities is evaluated from the ratio of photon fluxes, ε of H_δ to the Fulcher-α, namely,

$$\frac{\varepsilon(\mathrm{H}_\delta)}{\varepsilon(\mathrm{H}_2(d\rightarrow a))} = \frac{[\mathrm{H}]X_{1\rightarrow 6}^{\mathrm{eff}}(n_e,T_e)B(\mathrm{H}_\delta)}{n_e[\mathrm{H}_2]X_{d\leftarrow X}(T_e)} \tag{12}$$

where $X_{1\rightarrow 6}^{\mathrm{eff}}(n_e, T_e)$ is the effective cross-section for populating to the n = 6 state of the hydrogen atom, $B(\mathrm{H}_\delta)$ is the branching ratio of the radiative transition and $X_{d\leftarrow X}(T_e)$ is the total excitation rate of the Fulcher band based on the coronal model. Then, letting F = [H]/[H_2], the degree of dissociation can be represented as F/(F+2). Since the degree of dissociation is low in the present conditions (especially in the detached regime), the error or ambiguity in the determination of the molecular density based on Eq. (12), which is required for estimating the negative ion production, is negligible.

It should be noted that unlike in EIR plasmas, the H_γ/H_α or H_δ/H_α ratio, which is widely used in the divertor diagnostics in fusion devices [52], does not directly indicate the recombination in MAR plasmas. In the EIR plasmas, as will be seen in Sec. **4.1**, the population per degeneracy of n = 5 (H_γ) or 6 (H_δ) state is larger than that of the n = 3 (H_α) state. However, the electron temperature in the MAR plasmas is usually still in the ionizing regime.

3. Experimental Setup

3.1 Divertor/edge plasma simulator MAP-II

A dual-chamber steady-state linear divertor/edge plasma simulator, MAP-II, is schematically shown in Fig. 1(a). A longitudinal magnetic field of 15–20 mT is formed using 8 solenoid coils of 0.353 m in radius for the 90-turn larger coils and 0.154 m in radius for the 152-turn smaller ones. One of the smaller coils was replaced with a larger one in late 2002, when the device was moved to the Tokyo site of the Univ. Tokyo. As a result, the uniformity of the field in the target chamber has been improved, as can be seen in Fig. 1(b).

The detailed structure of the plasma source together with the discharge circuit is shown in Fig. 2. Power supplies (PS) for the main discharge are PS1 (250 V–20 A), PS2 (350 V–20

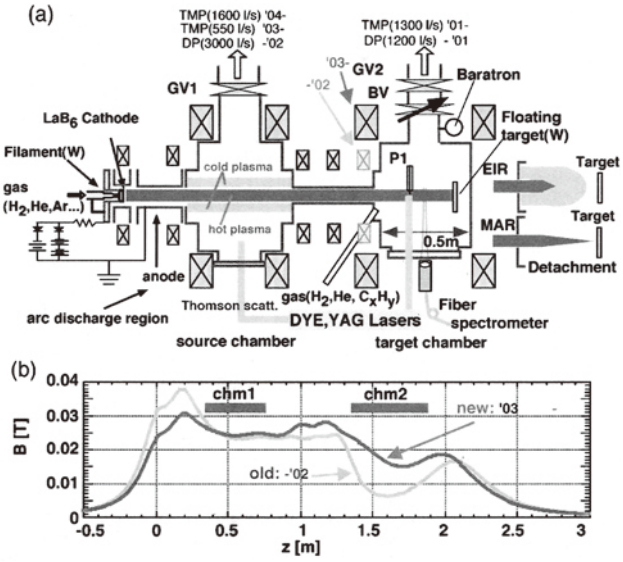

Fig. 1 (a) Schematic view of the MAP-II device. (b) Magnetic field strength of MAP-II. The seventh coil from the left was replaced to a large one in Dec. 2002.

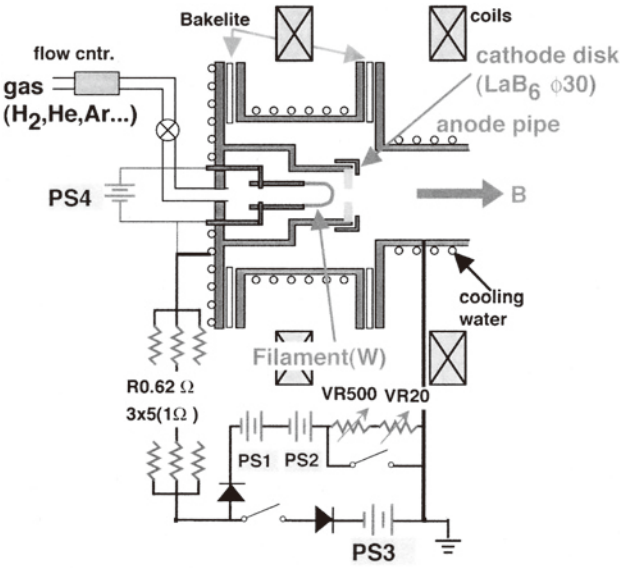

Fig. 2 Design of the plasma source and power supply circuit in MAP-II.

A) and PS3 (180 V–75 A). The former two are connected in series to each other and in parallel with PS3. This system satisfies the requirement both for glow and arc discharges. Each PS is electrically protected by means of a diode. A flat LaB_6 disk 30 mm in diameter having a hole 5 mm in diameter is used as a cathode while a water-cooled stainless steel nipple is used as an anode. The working gas, Ar, He or H_2 is injected into the source region through the hole in the cathode disk. Plasma is initiated by a glow discharge of about 200 mA at about 0.5–1 Torr. A typical discharge voltage for Ar, which is the most effective for the initial gas, is about 150 V, while the spark voltage is about 300–400 V. By controlling the variable ballast registers, transition to an arc discharge of about 40 V–1 A is achieved. This transition can be assisted by indirectly heating the cathode by means of a tungsten filament with a power of up to about 400 W. After the transition to the arc discharge, the current is further increased up to around 15 A, and then, the base pressure is reduced to several mTorr, which forms the core plasma stream with a diameter of about 5 cm. The working gas can be switched at this point if necessary. The discharge current can be further increased to the usual discharge condition of 30–50 A, while the resultant discharge voltage is 40–100 V, depending on the gas and the pressure.

The plasmas are transmitted through a first chamber (source chamber) into a second chamber (gas target chamber) at a distance of 1.5 m from the plasma source along a longitudinal magnetic field and terminated on the floating target plate.

The pump in the source chamber has been changed from a 3000 L/s diffusion pump (DP) to a 550 L/s turbo molecular pump (TMP) in 2003, and then recently to a 1600 L/s TMP, while that in the target chamber is a 1300 L/s TMP. For "attached" plasma conditions, in many cases, differential pumping operation is chosen in order to reduce the electron-neutral interactions [22]. To achieve a "detached" condition, however, it is easier if the pump for the source chamber is valved off, since this leads to a lowering of the electron temperature at the entrance of the target chamber to around 4–6 eV. Then, He, H_2 or Hydrocarbon gas can be puffed into the target chamber [53,54].

3.2 Diagnostics

A Langmuir probe system is used for electron density (n_e), temperature (T_e), and electron energy distribution function (EEDF) measurement. The EEDF can be modified to some extent by controlling the feed gas rate into the discharge region [55]. A Mach probe, slit probe (SP) and directional Langmuir probe (DLP) are used for the plasma flow measurement [56,57]. An L-shaped electrostatic probe is applied in a laser photodetachment (LPD) system for negative ion density measurements, which is combined with a dye laser pumped by second harmonic Nd:YAG laser pulses (532 nm) or with a Nd:YAG laser (532 or 1064 nm). Recently the laser has also been used for a Thomson scattering measurement [58,59].

A 1 m Czerny-Turner scanning monochromator was used for optical measurements. A 1200 grooves/mm brazed and 2400 grooves/mm holographic gratings can be selected. The spectrometer is equipped with dual output ports, one for the photo-multiplier tube (PMT) and the other for charge coupled device (CCD) detectors. The former is for the scanning spectrogram yielding a wider range of the spectra, and the latter is for the line-shape measurement such as ion temperature and flow velocity [60]. For the latter, astigmatism caused by the spherical mirrors is compensated for by using image expander optics equipped with two cylindrical lenses [61]. The typical wavelength resolution in the present work is less than 0.03 nm at a 50 μm slit width in the case of using the 2400 grooves/mm grating. The collection area of the emission can be varied depending on the object lens in front of the fiber-optical system.

In this series of experiments, a probe for the LPD is located about 5 cm upstream from the line-of sight for spectroscopy. The probe is also used for measurements of the general plasma parameters.

A list of diagnostics in the present MAP-II device and the typical plasma parameters measured by them are shown in Table 1.

Table 1 List of typical parameters in MAP-II and their diagnostics. $V_d(H^-)$ represent the drift velocity of the negative ions which corresponds to the thermal velocity v_{th} in the thermal equilibrium.

Source chamber	Parameter range	Diagnostics
n_e	0.9 – 30 × 10^{12} cm^{-3}	Thomson Scattering
T_e	1.5 – 10 eV	Thomson Scattering
T_e	0.06 eV (He-EIR)	He I CR model, Boltzmann plot.
T_i	0.8 – 1 eV	He II (n = 3–4) with fine structure
Target chamber	Parameter range	Diagnostics
n_e	10^{11} – 2 × 10^{12} cm^{-3}	Lamgmuir probe (attached), Double probe (detached)
T_e	3 – 15 eV 1 – 3 eV	Lamgmuir probe (attached), Double probe (detached)
T_e	0.05 eV (He-EIR)	He I CR model, Boltzmann plot.
T_i	0.4 – 0.7 eV	He II (n = 3–4) with fine structure
$M_{//}$ (Mach number)	0.1 – 0.2	Mach probe (MP), Slit probe (SP), and Directional Langmuir probe (DLP).
V_i (flow)	1.5 km/s	He II (n = 3–4) with fine structure
$[H^-]$	10^8 – 10^{10} cm^{-3}	LPD
$V_d(H^-) = v_{th}$	~ 10 km/s	LPD
p_0	0.8 – 20 mTorr	BARATRON gauge
T_{rot}	400 – 600 K	Fulcher spectroscopy
T_{vib}	2,000 – 10,000 K	Fulcher spectroscopy
Degree of dissociation	0.8 – 5 % (H_2-MAR)	Fulcher-Balmer ratio

4. Results and Discussion

4.1 Electron-ion recombination spectra

In this experiment, the discharge voltage and current were 71 V and 30 A, respectively. An EIR plasma can be achieved by valving off the differential pumping, operating with a little higher feeding rate of the working gas into the source region to achieve a higher base pressure and a lower electron temperature, and then puffing additional He gas into the target chamber. The base neutral pressure at the target chamber was set to 3.1 mTorr, which was measured using the BARATRON gauge. A small amount of hydrogen gas was seeded in the helium source gas, only a few percent, in order to observe the hydrogen Balmer series spectra. This hydrogen cannot affect the He discharge conditions.

The neutral pressure was increased up to 18 mTorr. A scanning spectrogram over the visible region was obtained and the atomic Boltzmann plot method was performed. The Rydberg spectra was observed, which indicated the EIR phase. As shown in Fig. 3, the slopes of the plot at the higher energy level are almost linear for both the He I triplet (a), He I singlet (b) and H I (c) cases.

The population of the excited state higher than n = 8 exhibits p-LTE. Considering the possible small uncertainty in the spontaneous emission coefficients in the Rydberg helium atom, T_e is deduced from the respective term series, namely 0.11 eV from (2^1P-n^1S, n = 9–11), 0.07 eV from (2^1S-n^1P, n = 9–11), 0.08 eV from (2^1P-n^1D, n = 9–14), 0.06 eV from (2^3P-n^3S, n = 9–13), and 0.07 eV from (2^3P-n^3D, n = 9–18). Wavelengths of the Rydberg spectra of the 2^3S-n^3P series are shorter than the lower limit of the spectroscopic system. It should be noted that the Hydrogen Balmer series up to n = 13 is also observed [36].

The electron temperature determined from the hydrogen Rydberg series (n = 9–13) was revealed to be 0.06 eV, showing a similar value to that from the He series, which confirms the achievement of the p-LTE.

As mentioned in Sec. **2.1.2**, however, the lowest state used in the Boltzmann plot method is sometimes not clear. We have therefore applied the CR-model for HeI to the EIR plasmas. The electron temperature and density are determined from the best-fit of the CR-model to the experimental data. Since series spectra can be observed up to a highly excited state in EIR plasmas, the accuracy of the fitting is reliable as can be seen in Fig. 4. It should be noted that the radiation trapping should be taken into account even for using a triplet series to obtain density, since a collisional redistribution between the singlet and the triplet series has a significant contribution to the population coefficients [62]. On the other hand, the modification of the deduced electron temperature due to radiation trapping is negligible. For the dimension of the system, L, in the optical escape factor, in our condition, the radius of the hot plasma column 25 mm was used. Figure 5(a) shows the comparison of the distribution calculated based on the Boltzmann plot with that based on the CR model for the triplet-D series. One can see that, in the study of the EIR plasmas, p-LTE may be a substantially good approximation

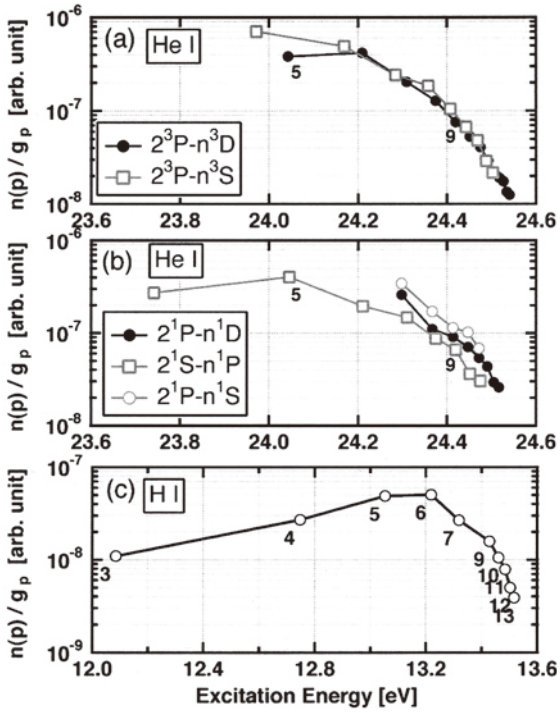

Fig. 3 Boltzmann-plots (population per degeneracy for the $n = p$ state) of (a) He I triplet series, (b) He I singlet series, and (c) H I. The p-LTE is achieved above the principal quantum number of around n = 9. [Shot# 13256-13259]

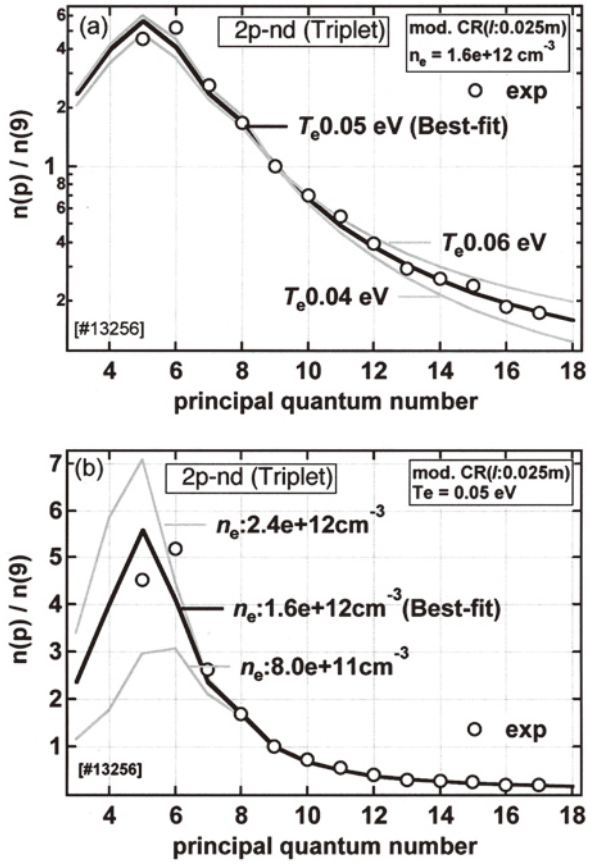

Fig. 4 Fitting of the CR model calculations to the experimental data for ^{3}D series. (a) is for determining T_e while (b) is for determining n_e assuming an absorption length l = 0.025 m. [Shot# 13256-13259]

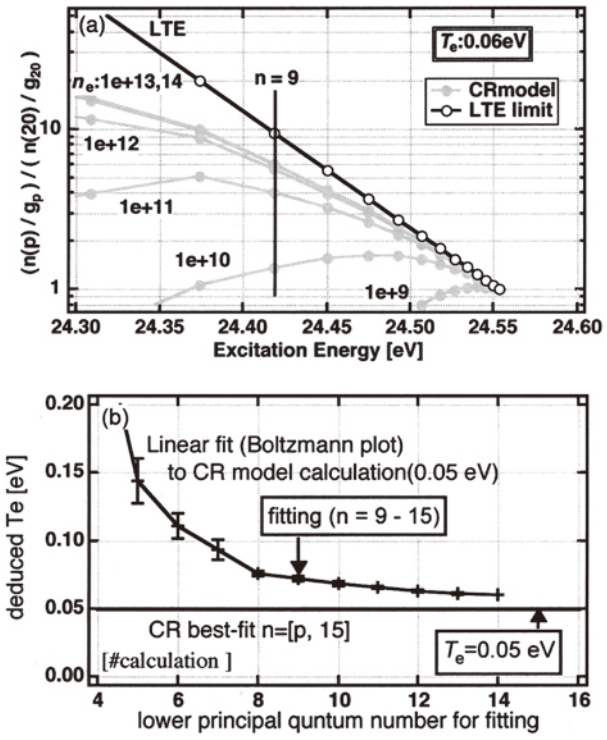

Fig. 5 (a) Comparison of the distribution calculated based on the Boltzmann plot with that based on the CR-model for ^{3}D series. (b) Possible deviation of the results of the Boltmann plot from that calculated based on the CR-model.

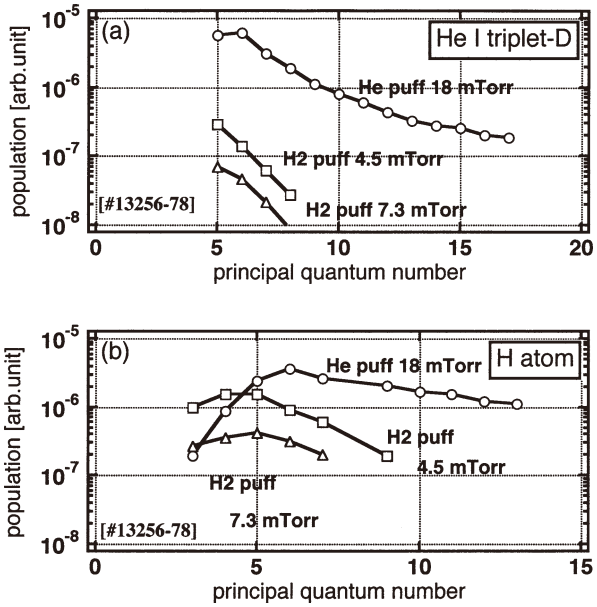

Fig. 6 Relative distribution of the excited state population of (a) He I triplet D, (b) He I singlet P and (c) H I for the different gas puffing condition. Base Helium pressure is 3.1 mTorr and the puffing gas and the total pressures for each case are appended. [Shot# 13256-13278]

provided $n_e \geq 10^{12}$–10^{13} cm^{-3}, while it is better to use the CR model for lower density. In order to evaluate the quantitative deviation of the Boltzmann plot method from the CR model, we performed the Boltzmann plot on the population distribution of the triplet-D series reproduced based on the CR model for T_e = 0.05 eV. Although the deviation depends on the electron density and temperature, one can see from Fig. 5(b) quantitatively that T_e from the Boltzmann plot approaches that from the CR-model as the lowest value of n increases. The difference is rather small for $n \geq 9$ where the spectral intensity becomes weaker and the interval becomes narrower. If the error in the intensity is large and the number of the levels is limited, the CR model provides more reliable values of T_e. Furthermore, at least rough values of n_e can also be obtained using the CR model, if an appropriate absorption length is assumed.

It should be noted that the Boltzmann distribution for the electrons is assumed in the collisional excitation rates in the CR models. On the other hand, it is difficult to determine the EEDF in recombining plasmas, since the probe cannot be applied due to the anomaly. However, the fact that the Boltzmann plot method (not affected by the excitation rate) and the CR model calculation (dominated by the collisional processes) give the same electron temperature implies that the bounded electrons in the Rydberg states achieve equilibrium with the free electrons through collisional processes. Therefore, we think that the Boltzmann EEDF is a good approximation in a practical sense, at least in the Rydberg states where T_e can be deduced. This should be confirmed in a future study.

4.2 Study of hydrogen-MAR processes

Figure 6 shows the relative population density in the excited state as a function of the principal quantum number in the cases of He puff to achieve He-EIR (18 mTorr), H_2 puff to achieve weak MAR (4.5 mTorr), and H_2-puff to achieve stronger H_2-MAR (7.3 mTorr). Note that the ion flux measured in the target chamber is almost equal for He-EIR (18 mTorr) and weak H_2-MAR as can be seen in Fig. 7(a). As seen in Fig. 6, the Rydberg series population observed in the EIR plasma completely disappears in the case of hydrogen puffing, and the line emission is no longer in the p-LTE, as reported by Ohno *et al.* [63]. At the same time, negative hydrogen ions can be observed in the peripheral region of the plasma stream, as shown in Fig. 7(b), where the electron temperature is expected to be low. One should bear in mind that, in this series of experiments in 2003, only a single Langmuir probe was used, so that the obtained values of T_e, and consequently n_e were not reliable due to the anomalous probe characteristics as mentioned in Sec. **1**. We assumed T_e = 1 eV and used Eq. (4) for a rough estimate of the negative ion density.

This ambiguity in the determination of the negative ion density has been resolved in 2004 by mounting the double probe on the same probe head as the L-shaped probe for LPD, as mentioned in Sec. **2.2.2**. Therefore quantitative discussions of the production-depletion balance of the negative ion become possible together with the vibrational temperature measured by Fulcher spectroscopy.

Figure 8 shows the dependence of the measured parameters on gas pressure. As the H_2-MAR processes proceed,

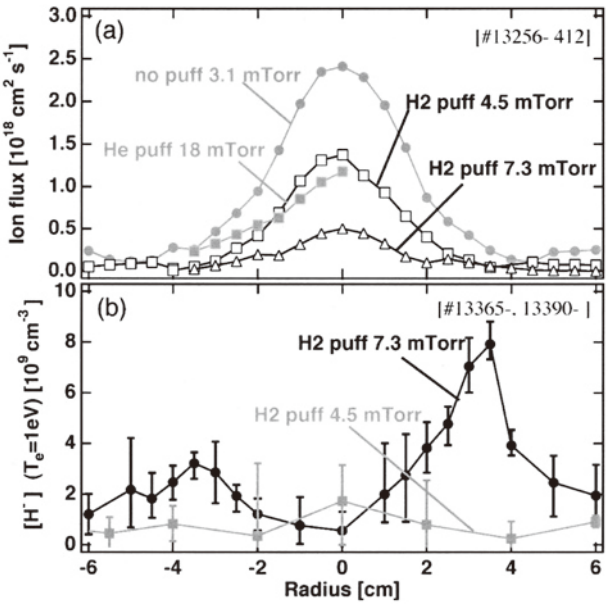

Fig. 7 (a) Reduction of the ion flux induced by the recombination processes. (b) Negative ion density deduced assuming T_e = 1 eV, since T_e could not be measured by a single Langmuir probe. [Shot# 13256-13412]

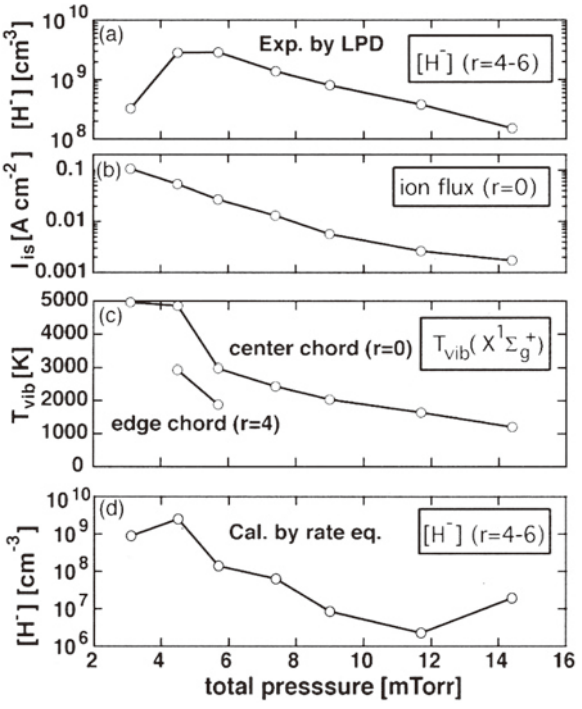

Fig. 8 Pressure dependence of the measured quantities. (a) Negative ion density averaged over r = 4–6 cm. T_e was measured by a double probe. (b) The ion saturation current at r = 0 cm. (c) The vibrational temperature for central and edge chords. (d) Calculated negative ion density based on the rate equation. [Shot# 17734-17868]

negative ion density averaged over the peak position r = 4–6 cm (a) exhibits a remarkable decrease. The initial increase is attributed to the initial injection of the H_2 gas. The remarkable decrease in the ion saturation current (b) as the hydrogen gas increases indicates the onset of the MAR processes. This was previously described in ref. [54] where a comparative investigation was made between the case of He, H_2 and hydrocarbon puffing into the He background plasma stream. We have checked in ref. [38] that T_e does not change so much over this pressure range, implying that the reduction of the ion flux corresponds mainly to that of the electron density. Both results indicate that the ratio of the negative ion density to the electron density is almost constant during this MAR phase.

In order to clarify the behaviors of the negative ions in the H_2-MAR plasmas, we evaluated the negative ion density from a steady state solution of the following simple rate equation [34,38]:

$$\frac{dn_{H^-}}{dt} + \nabla \cdot (n_{H^-} v_d) = n_e \sum_{0 \le v \le 9} \alpha_{e,H_2} n_{H_2(v)} - n_{H^-} \left(n_{H^+} \alpha_{H^+,H^-} + n_e \alpha_{e,H^-} \right), \quad (13)$$

where α_{e,H_2}, α_{H^+,H^-} and α_{e,H^-} are the rate coefficients for dissociative attachment (DA), mutual neutralization (MN) and electron impact detachment (EDet), respectively [64-66]. We assumed in the equation that the vibrational distribution of H_2 in the ground electronic state is Boltzmann, namely that it can be characterized by T_{vib}, and that the MN rates for H_2^+ and He^+ are equal to that of H^+. We first neglect the contribution from the transport term and discuss it later.

As input parameters, T_{vib} and H_2 density were measured as a function of the total neutral pressure together with the routine plasma parameters, such as n_e or T_e. The hydrogen molecular density was deduced from the total pressure measured with a BARATRON gauge, the helium partial pressure measured with quadrupole mass analyzer (QMA), and a Fulcher-Balmer ratio described in Eq. (12). As seen from the comparison between Fig. 8(a) and (d), measured negative ion density is on the same order with the calculations in the initial part, while the calculation results show considerably lower density as the pressure increases.

As reported in ref. [38], we suspected that the negative ions in the MAR condition are mainly produced in the core region and transported *to* the periphery without encountering destruction processes such as MN or EDet. On the other hand, in the attached condition, reported in ref. [34], transport loss *from* the peripheral region should be taken into consideration to reproduce the negative ion density.

The lifetime of the negative ions can be estimated from the reciprocal of the destruction rate. Figure 9 shows the comparison of the destruction rate between the attached and detached conditions for the negative ions at the center of the plasma column. The data in both conditions have been reported in refs. [34] and [38], respectively. Even at the same pressure in the gas target chamber, the electron density and temperature are different depending on the operation conditions. In the initial condition of the MAR, the lifetime is about a few μs which is comparable to that in the attached case. However, as the H_2-MAR process proceeds, the lifetime

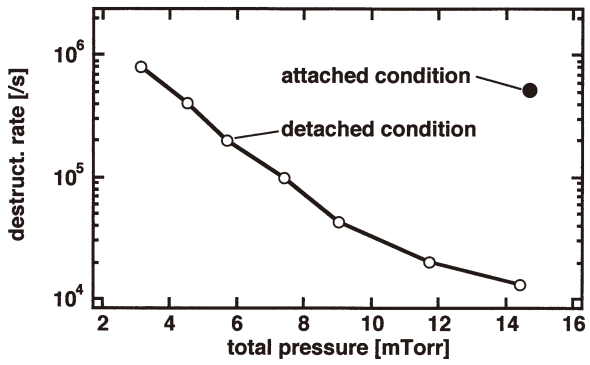

Fig. 9 Comparison of the destruction rate of the negative ions produced at the center of the plasma column between attached [34] and detached [38] conditions. The reciprocal of the value represents the lifetime of the negative ions.

is greatly lengthened. The drift velocity of the negative ions deduced from the temporal waveforms of the LPD signals [37] is on the order of several km/s, yielding a travel distance of at least several cm. This characteristic scale length increases as the H_2-MAR process proceeds, which does not contradict the qualitative observations. Kinetic treatments or particle simulations are necessary for more qualitative discussions including the radial profiles of the production, destruction and transport effects. These topics will be subjects of study in the future.

Another possible reason for the discrepancy is the departure from a Boltzmann distribution of the vibrational distribution function in the ground electronic state of the hydrogen molecules. As can be understood from the Franck-Condon factors for the *X-d* excitation in the H_2 molecule, the Fulcher-α band is sensitive to the vibrational distribution for $v \leq 4$, while the main contributor to the negative ion production is the population in $v \geq 4$. Therefore, if a "tail", "bi-Maxwellian" or "plateau" region exists in the vibrational distribution in the ground electronic state, the production cannot be predicted from the Fulcher band spectroscopy on the basis of the T_{vib}. Our kinetic modeling for the mechanism of the vibrational distribution [67], as well as several calculations and LIF measurements [68], indicates a departure from a Boltzmann distribution. Our recent results from the Fulcher-band spectroscopy indicate that, when increasing the H_2 pressure in the MAR plasmas, the deduced T_{vib} depends greatly on the input values of T_e in the analysis, whereas the observed intensity ratio of the vibronic transitions are not so greatly changed. This may be the possible reason for the non-thermalized feature of the vibrational distribution in the ground electronic state. This should also be investigated in the future.

5. Summary and Future Prospects

We have reviewed the measurement techniques which can be used for the study of the volumetric recombining plasmas dominated by He-EIR and/or H_2-MAR. Quantitative comparison between the Boltzmann plot method and the CR-model were made in the He-EIR plasmas. T_e obtained by both methods agrees well in the considerably high density region, while the absorption scale length of the 1^1S-n^1P series should be taking into account for the determination of the electron density even when using the triplet series. In the study of the H_2-MAR, negative hydrogen ion density, vibrational temperature of the hydrogen molecules, and molecular density were measured at the same time. Then, the measured negative ion density was compared with the theoretical calculation based on the rate equation without the transport term. Transport effects were discussed both in the attached and detached conditions and we concluded that the magnitude of the destruction rate and the travel distance are the key factors to understand this. Kinetics of the negative ion behavior and/or the non-equilibrium feature of the vibrational distribution of the molecular hydrogen might be clarified by further investigation.

Moreover, the contribution of molecular ions such as H_2^+, H_3^+ and HeH^+ or of hydrocarbon radicals to the MAR processes also needs to be clarified for a complete understanding of the atomic and molecular processes relevant to the diverter detachment. We believe that this can lead not only to the useful monitoring of the divertor plasmas but also to the proposal of an effective scenario for divertor operation to mitigate the particle and heat loads to the divertor plates [54,69].

Acknowledgements

The first and second authors wish to acknowledge Dr. Goto in NIFS for the useful code of CR model for He I. This work was supported in part by NIFS Collaborative Research Program (NIFS04KOAB009) and by TEPCO research foundation.

References

[1] O. Gruber, A. Kallenbach *et al.*, Phys. Rev. Lett. **74**, 4217 (1995).
[2] S.I. Krasheninnikov, A. Yu. Pigarov and D.J. Sigmar, Phys. Lett. A **214**, 285 (1996).
[3] R.K. Janev, T. Kato and J.G. Wang, Phys. Plasmas **7**, 4364 (2000).
[4] R.D. Monk *et al.*, J. Nucl. Mater. **241-243**, 396 (1997).
[5] N. Ezumi *et al.*, Contrib. Plasma Phys. **38**, S31 (1998).
[6] N. Ohno *et al.*, Contrib. Plasma Phys. **41**, 473 (2001).
[7] E.M. Hollmann, G. Antar, R.P. Doerner and S.C. Luckhardt, Rev. Sci. Instrum. **72**, 623 (2001).
[8] D.G. Whyte, R.P. Seraydarian and R.P. Doerner, J. Vac. Sci. Technol. A **17**, 2713 (1999).
[9] W. Bohmeyer, D. Naujoks, A. Markin, I. Arkhipov, B. Koch, D. Schröder and G. Fussmann, J. Nucl. Mater. **337-339**, 89 (2005).
[10] A.M. Litnovsky, B.I. Khripunov, G.V. Sholin, V.B. Petrov, V.V. Shapkin and N.V. Antonov, J. Nucl. Mater. **290-293**, 1107 (2001).
[11] P.K. Browning, U. Fantz, K.J. Gibson, B. Mihaljcic and D. Wunderlich, J. Nucl. Mater. **337-339**, 232 (2005).
[12] A. Matsubara, T. Watanabe, T. Sugimoto, S. Sudo and K. Sato, J. Nucl. Mater. **337-339**, 181 (2005).

[13] N. Ohno, S. Uno, Y. Hirooka and S. Takamura, J. Nucl. Mater. **290-293**, 299 (2001).
[14] N. Ohno, Y. Kobayashi, T. Sugimoto and S. Takamura, J. Nucl. Mater. **337-339**, 35 (2005).
[15] A. Tonegawa, M. Ono, Y. Morihira, H. Ogawa, T. Shibuya, K. Kawamura and K. Takayama, J. Nucl. Mater. **313-316**, 1046 (2003).
[16] H. Bolt and S. Tanaka, J. Nucl. Mater. **191-194**, 364 (1992).
[17] H. Bolt, V. Hemel, H. Nickel and S. Tanaka, Surface and Coatings Tech. **74-75**, 188 (1995).
[18] S. Matsuyama, K. Yamaguchi, S. Tanaka and M. Yamawaki, J. Nucl. Mater. **233-237**, 648 (1996).
[19] S. Matsuyama, K. Yamaguchi, S. Tanaka and M. Yamawaki, Fusion Eng. Design **34-35**, 763 (1997).
[20] S. Matsuyama, K. Yamaguchi, S. Tanaka and M. Yamawaki, Fusion Eng. Design **39-40**, 393 (1998).
[21] K. Kobayashi, S. Ohtsu and S. Tanaka, J. Nucl. Mater. **266-269**, 850 (1999).
[22] K. Kobayashi, S. Kado, B. Xiao and S. Tanaka, J. Nucl. Mater. **290-293**, 648 (2001).
[23] D. Nishijima, *et al.*, Plasma Phys. Control. Fusion **44**, 597 (2002).
[24] D. Lumma, J.L. Terry and B. Lipshultz, Phys. Plasmas **4**, 2555 (1997).
[25] T. Fujimoto, J. Quant. Spectrosc. Radiat. Transfer **21**, 439 (1979).
[26] M. Goto, J. Quant. Spectrosc. Radiat. Transfer **76**, 331 (2003).
[27] M. Otsuka, R. Ikee and K. Ishii, J. Quant. Spectrosc. Radiat. Transfer **21**, 41 (1979).
[28] R.K. Janev, D.E. Post, W.D. Langer, *et al.*, J. Nucl. Mater. **121**, 10 (1984).
[29] R. Janev, Physica Scripta **T96**, 94 (2002).
[30] R.F.G. Meulenbroeks, *et al.*, Phys. Rev. E **49**, 4397 (1994).
[31] J.L. Terry, B. Lipschultz, A.Yu. Pigarov, S.I. Krasheninnikov, B. LaBombard, D. Lumma, H. Ohkawa, D. Pappas and M. Umansky, Phys. Plasmas **5**, 1759 (1998).
[32] M. Bacal, G.W. Hamilton, A.M. Bruneteau and H.J. Doucet, Rev. Sci. Instrum. **50**, 719 (1979).
[33] M. Bacal, Rev. Sci. Instrum. **71**, 3981 (2000).
[34] S. Kajita, S. Kado, N. Uchida, T. Shikama and S. Tanaka, J. Nucl. Mater. **313-316**, 748 (2003).
[35] S. Kajita, S. Kado, T. Shikama, B. Xiao and S. Tanaka, Contrib. Plasma Phys. **44**, 607 (2004).
[36] S. Kado, S. Kajita, Y. Iida, B. Xiaoa, T. Shikama, D. Yamasaki, T. Oishi and S. Tanaka, Plasma Sci. Technol. **6**, 2451 (2004).
[37] S. Kajita, S. Kado, A. Okamoto and S. Tanaka, Phys. Rev. E. **70**, 066403 (2004).
[38] S. Kado, S. Kajita, D. Yamasaki, Y. Iida, B. Xiao, T. Shikama, T. Oishi, A. Okamoto and S. Tanaka, J. Nucl. Mater. **377-379**, 166 (2005).
[39] S. Kajita, S. Kado, A. Okamoto and S. Tanaka, Jpn. J. Appl. Phys, *in press*.
[40] S. Kajita, S. Kado and S. Tanaka, Plasma Sources Sci. Technol. **14**, 566 (2005).
[41] M. Nishiura, J. Plasma Fusion Res. **80**, 757 (2004).
[42] B.P. Lavrov, Opt. Spectrosc. **48**, 375 (1980).
[43] U. Fantz and B. Heger, Plasma Phys. Control. Fusion **40**, 2023 (1998).
[44] U. Fantz, K. Behringer, J. Gafert, D. Coster and ASDEX Upgrade Team, J. Nucl. Mater. **266-269**, 490 (1999).
[45] N. Ginsburg and G.H. Dieke, Phys. Rev. **59**, 632 (1941).
[46] B. Xiao, S. Kado, S. Kajita and D. Yamasaki, Plasma Phys. Control. Fusion **46**, 653 (2004).
[47] N.N. Sobolev, *Electron-excited molecules in non-equilibrium plasma*. (Nova Science Publishers, NewYork, 1989) p. 121-173.
[48] M. Gryzinski, Phys. Rev. **138** (2A) A336-A358.
[49] S. Kado, D. Yamasaki, Y. Iida and B. Xiao, J. Plasma Fusion Res. **80**, 783 (2004) [*in Japanese*].
[50] S. Kado, D. Yamasaki, Y. Iida and B. Xiao, *to be published in* J. Plasma Fusion Res. SERIES (2005).
[51] T. Fujimoto, K. Sawada and K. Takahata, J. Appl. Phys. **66**, 2315 (1989).
[52] G.M. McCracken, R.D. Monk, A. Meigs, L. Horton, L.C. Ingesson, J. Lingertat, G.F. Matthews, M.G. O'Mullane, R. Prentice, M.F. Stamp and P.C. Stangeby, J. Nucl. Mater. **266-269**, 37 (1999).
[53] H. Kobayashi, S. Kado, B Xiao and S. Tanaka, Jpn. J. Appl. Phys. **42**, 1776 (2003).
[54] S. Kado, H. Kobayashi, T. Oishi and S. Tanaka, J. Nucl. Mater. **313-316**, 754 (2003).
[55] T. Shikama, S. Kado, S. Kajita and S. Tanaka, Jpn. J. Appl. Phys. **43**, 809 (2004).
[56] T. Shikama, S. Kado, A. Okamoto, S. Kajita and S. Tanaka, J. Nucl. Mater. **337-339**, 1077 (2005).
[57] T. Shikama, S. Kado, A. Okamoto, S. Kajita and S. Tanaka, Phys. Plasmas **12**, 044504 (2005).
[58] A. Okamoto, S. Kado, N. Fukuzawa *et al.*, *proc. Plasma Science Symposium 2005/ The 22nd Symposium on Plasma Processing* (PSS-2005/SPP-22) (2005.1.26-28, Nagoya, Japan) P1-022, 69 (2005).
[59] A. Okamoto, S. Kado, S. Kajita and S. Tanaka, *to be published in* Rev. Sci. Instrum.
[60] S. Kado, T. Shikama, S. Kajita, T. Oishi and S. Tanaka, Contrib. Plasma Phys. **44**, 656 (2004).
[61] S. Kado and T. Shikama, J. Plasma Fusion Res. **79**, 841 (2003).
[62] Y. Iida, S. Kado, A. Okamoto, S. Kajita, T. Shikama, D. Yamasaki and S. Tanaka, *to be published in* J. Plasma Fusion Res. SERIES (2005).
[63] N. Ohno, N. Ezumi, S. Takamura *et al.*, Phys. Rev. Lett. **81**, 818 (1998).
[64] R. Celiberto, R.K. Janev, A. Laricchiuta, M. Capitelli, J.M. Wadehra and D.E. Atems, Atomic Data and Nuclear Data Tables **77**, 161 (2001).
[65] J.M. Wadehra, Appl. Phys. Lett. **35**, 917 (1979).

[66] R.K. Janev, W.D. Langer *et al.*, *Elementary Processes in Hydrogen-Helium Plasmas* (Springer, 1987).
[67] B. Xiao, S. Kado, S. Kajita, D. Yamasaki and S. Tanaka, J. Nucl. Mater. **377-379**, 1082 (2005).
[68] T. Mosbach, H.M. Katsch and H.F. Döbele, Phys. Rev. Lett. **85**, 3420 (2000).
[69] T. Nakano and S. Kado, J. Plasma Fusion Res. **80**, 91 (2004). [*in Japanese*]